Ultrafast Primary Processes in Photosystem I of the Cyanobacterium *Synechocystis* sp. PCC 6803

Sergei Savikhin,* Wu Xu,# Victor Soukoulis,* Parag R. Chitnis,# and Walter S. Struve*
*Ames Laboratory–U.S. Department of Energy, Department of Chemistry, and #Department of Biochemistry and Biophysics, Iowa State University, Ames, Iowa 50011 USA

ABSTRACT Ultrafast primary processes in the trimeric photosystem I core antenna-reaction center complex of the cyanobacterium *Synechocystis* sp. PCC 6803 have been examined in pump-probe experiments with ~100 fs resolution. A global analysis of two-color profiles, excited at 660 nm and probed at 5 nm intervals from 650 to 730 nm, reveals 430 fs kinetics for spectral equilibration among bulk antenna chlorophylls. At least two lifetime components (2.0 and 6.5 ps in our analysis) are required to describe equilibration of bulk chlorophylls with far red-absorbing chlorophylls (>700 nm). Trapping at P700 occurs with 24-ps kinetics. The multiphasic bulk ↔ red equilibration kinetics are intriguing, because prior steady-state spectral studies have suggested that the core antenna in *Synechocystis* sp. contains only one red-absorbing chlorophyll species (C708). The disperse kinetics may arise from inhomogeneous broadening in C708. The one-color optical anisotropy at 680 nm (near the red edge of the bulk antenna) decays with 590 fs kinetics; the corresponding anisotropy at 710 nm shows ~3.1 ps kinetics. The latter may signal equilibration among symmetry-equivalent red chlorophylls, bound to different monomers within trimeric photosystem I.

INTRODUCTION

Primary processes in the core antenna-reaction center complexes of PS I in cyanobacteria and green plants have been widely studied by ultrafast spectroscopy since the mid-1980s (van Grondelle et al., 1994). Several models have been proposed for global energy transfers among the relevant Chl *a* antenna pigment pools and reaction center (e.g., Holzwarth, 1992; Jia et al., 1992; Hastings et al., 1995). Before 1993, molecule-specific insights into the energy transfers were precluded by the lack of a crystal structure and the unavailability of stable femtosecond lasers in the visible region (650–750 nm) of Chl *a* Q_y absorption spectra. The appearance of a 3-dimensional structure of the PS I core antenna-reaction center complex from the cyanobacterium *Synechococcus elongatus* (Krauss et al., 1993, 1996) has prompted an enormous resurgence of interest in this system. We have recently built a Ti:sapphire laser system with regenerative amplifier and optical parametric amplifier, which yields tunable visible output when frequency-doubled. Its time resolution and stability emulate the performance of infrared Ti:sapphire lasers (700–1000 nm), which have already been widely exploited in studies of LH1/LH2 antennas of purple bacteria (Pullerits and Sundström, 1996), FMO trimers from green sulfur bacteria (Buck et al., 1997; Vulto et al., 1997), and chlorosomes from green thermophilic and sulfur bacteria (Savikhin et al., 1994, 1995). Our present combination of pulse-to-pulse stability and pulse duration (70–90 fs) at these wavelengths affords fresh glimpses into the femtosecond and picosecond primary processes in PS I.

Prior knowledge of PS I antenna-reaction center processes, accumulated since the mid-1980s via steady-state and time-resolved spectroscopy, has been summarized by van Grondelle et al. (1994). The P700 reaction center is surrounded by ~100 Chl *a* core antenna pigments, which are dispersed over several spectral forms with Q_y absorption maxima ranging from ~660 to ~685 nm (Ikegami and Itoh, 1985; Owens et al., 1988; Jia et al., 1992; van der Lee et al., 1993; Gobets et al., 1994). Some 80 of these "bulk" antenna Chls are discernible in the 4 Å x-ray structure of Krauss et al. (1996). Spectroscopic evidence points to the existence of a much smaller pool of "red" antenna Chls (2–5 pigments), absorbing at longer wavelengths than the P700 absorption band. Gobets et al. (1994) reported that *Synechocystis* sp. PCC 6803 has two Chls absorbing at 708 nm (hereafter denoted C708). The number and types of such red Chls apparently depend on species; Holzwarth (1992) detected four 712-nm Chls and one 725-nm Chl through Gaussian deconvolution of room-temperature absorption spectra in *Synechococcus*. According to Shubin et al. (1992), *Spirulina* has one or more Chls absorbing at 730 nm. It has been suggested that such "red" Chls lie close to the reaction center and serve to focus bulk antenna excitation toward the reaction center (Werst et al., 1992; Jia et al., 1992; Trinkunas and Holzwarth, 1994). However, recent evidence (Karapetyan et al., 1997) suggests that (some of) the red Chls may lie on the PS I periphery, rather than adjacent to the reaction center.

Received for publication 16 October 1998 and in final form 16 March 1999.

Address reprint requests to Dr. Walter S. Struve, Dept. of Chemistry, Iowa State University, Gilman Hall, Ames, IA 50011-3111. Tel.: 515-294-4276; Fax: 515-294-1699; E-mail: wstruve@ameslab.gov.

Abbreviations used: PS I, photosystem I; Chl, chlorophyll; DAS, decay-associated spectrum; ESA, excited state absorption; OPA, optical parametric amplifier; PB, photobleaching; P700, primary electron donor in photosystem I; SE, stimulated emission.

0006-3495/99/06/3278/11 $2.00

Equilibration among bulk Chl spectral forms (660–690 nm) is unresolvable under the picosecond resolution of photon counting and most dye laser absorption difference experiments. Evidence for ~200 fs downhill energy transfer steps within the bulk antenna emerged in a fluorescence upconversion study (Du et al., 1993). Hastings et al. (1995) concluded that bulk ↔ red Chl equilibration occurs with 3.7–7.5 ps kinetics, depending on species. In core antenna-reaction centers from *Synechocystis* sp. PCC 6803, this process requires 2.7–4.3 ps, and the subsequent trapping at P700 occurs during the next 19–24 ps. Marked discrepancies have appeared among the kinetics reported for these steps by other groups, working with several different preparations [e.g., from *Chlamydomonas* (Du et al., 1993), *Synechocystis* (Hecks et al., 1994), and *Synechococcus* (Holzwarth et al., 1993; Turconi et al., 1993)]. Hastings et al. (1995) discerned only minor species variations in these lifetimes, and suggested that the discrepancies arise principally from differences in experimental technique.

In this paper we reinvestigate the excitation transfer and trapping processes in PS I of wild-type *Synechocystis* sp. PCC 6803. Our resolution of <100 fs allows us to observe well-defined femtosecond spectral equilibration within the Chl *a* bulk antenna. Our combination of laser stability and time resolution allows us to differentiate at least two lifetimes for equilibration between bulk and red antenna Chls (2 and 6.5 ps), with decay-associated growth spectra peaking near 705 and 720 nm, respectively. This result is particularly interesting, because Gobets et al. (1994) reported that *Synechocystis* sp. exhibits only one red spectral form (C708), whose low-temperature fluorescence maximum (720 nm) is anomalously red-shifted by 200 cm^{-1} from the absorption peak (versus ~80 cm^{-1} for monomeric Chl; Kwa et al., 1994). Our results show that the red Chls attain quasiequilibrium with the bulk antenna, with the result that excitations decay with ~24 ps kinetics in all Chl spectral forms at long times (red as well as bulk). Singlet-singlet annihilation sets in for laser fluences corresponding to excitation of 1 of ~120 Chls, which is roughly the Chl content of monomeric PS I. The bulk and red antennas show fundamentally different anisotropy behavior, with contrasting lifetimes and final anisotropies.

MATERIALS AND METHODS

Trimeric PS I complexes were purified from the wild-type strain of the cyanobacterium *Synechocystis* sp. PCC 6803 by a previously published method (Sun et al., 1998). Optical clarity of the PS I preparation was improved by centrifugation through Spin-X centrifuge filter units (0.22 μm cellulose acetate membrane; Costar). The chlorophyll concentration of PS I trimers was measured in 80% acetone. Purity of PS I preparations was examined by SDS-PAGE analysis of protein subunits.

A self-mode-locked Ti:sapphire laser (pumped by a 5W multiline Coherent Radiation Innova 90-5 argon ion laser) generated 780 nm pulses with 50–80 fs duration at 100 MHz repetition rate. These were passed through an optical isolator and dispersed to ~150 ps duration in a grating pulse stretcher. The pulses were then amplified by a factor of ~10^6 at 1 kHz (0.5 mJ/pulse) in a Ti:sapphire regenerative amplifier, pumped by a Clark-MXR ORC-1000 Q-switched Nd:YAG laser (Dexter, MI). The regenerative amplifier incorporated a Medox Electro-Optics Pockels cell. After recompression to 90–100 fs duration in a dual grating pulse compressor, the amplified pulses were converted in a type I BBO OPA crystal into infrared signal and idler frequencies ($\omega \rightarrow \omega_1 + \omega_2$). The OPA design, after that of Hasson (1997), employed a double-pass configuration; the OPA process was initiated by continuum seed pulses generated by focusing <1% of the 780 nm pulses into a sapphire crystal. This seeding greatly increased the signal/noise in the OPA signal pulses. Frequency-doubling the OPA signal output pulses yielded visible light pulses that were easily tunable over the entire PS I Chl *a* Q_y spectrum (600–720 nm). Aside from the argon ion and Nd:YAG pump lasers, all major optical assemblies (including the regenerative amplifier) were built in-house. A Gaussian fit to a Kerr-effect cross-correlation profile between 680 nm frequency-doubled signal pulses and 700 nm broadband continuum pulses generated in a sapphire plate yielded 98 fs fwhm (Fig. 1), which would correspond to 70 fs fwhm laser pulses if the signal and continuum pulse profiles had identical shapes. Cross-correlations at other wavelengths varied from 100 to 200 fs fwhm. Due to group velocity dispersion in the optics, the timing between pump and probe pulses varied with wavelength (by ~400 fs for probe wavelengths between 650 and 730 nm); this was calibrated for all combinations of pump and probe wavelengths.

For pump-probe experiments, frequency-doubled OPA signal pulses served as pump pulses, while the broadband continuum pulses sampled the PS I ΔA spectrum at variable time delays. Continuum pulses were split into reference and probe beams; both were focused into the PS I sample cell, but only the probe beam intersected the pump beam. The reference and probe beams were dispersed in a programmable Oriel MS257 imaging monochromator with 1200 groove/mm grating operated at ~2 nm bandpass, and directed onto separate Hamamatsu S3071 Si pin photodiodes (5 mm diameter active area). The photodiode signals for every pulse were integrated in Stanford Research Systems SR250 boxcar integrators, and digitized in a National Instruments MIO-000 16-bit analog-to-digital converter (ADC) computer plug-in module. The time delay sweep and monochromator drive were automated with Spectra-Solve software (Ames Photonics, Inc., Ames, IA), and a ΔA surface versus time and probe wavelength (e.g., 15 probe wavelengths from 660 to 700 nm) could be generated in ~2 h without realignment of lasers or optics (Fig. 2). The laser was stabilized to the extent that ΔA signals were measurable down to ~5×10^{-5} with signal averaging over 1 s (10^3 pulses); probe/reference beam fluctuations were as low as 0.1–0.2% rms. The noise performance was limited chiefly by the photodiode preamplifiers and boxcar integrators. Photosystem I samples were housed in ~0.7 mm path length, 2-inch diameter centrifugal cells rotating at ~10 Hz; given the 1 kHz laser repetition rate, successive pulses excited nonoverlapping spots in the cell. The PS I optical density was typically ~0.4 at 680 nm. Unless otherwise specified, experiments were

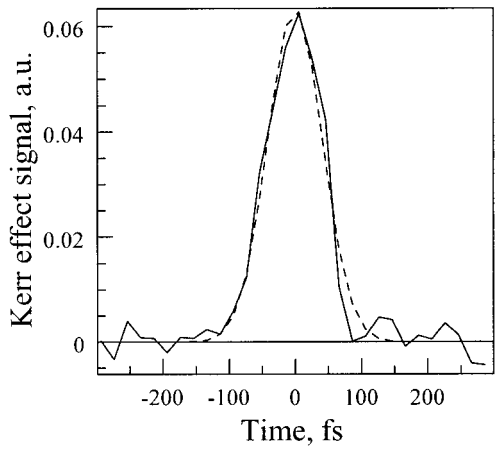

FIGURE 1 Kerr-effect cross-correlation between 680 nm frequency-doubled OPA output and broadband continuum viewed at 700 nm with 2 nm bandpass (*solid curve*); 98 fs fwhm Gaussian fit (*dashed curve*).

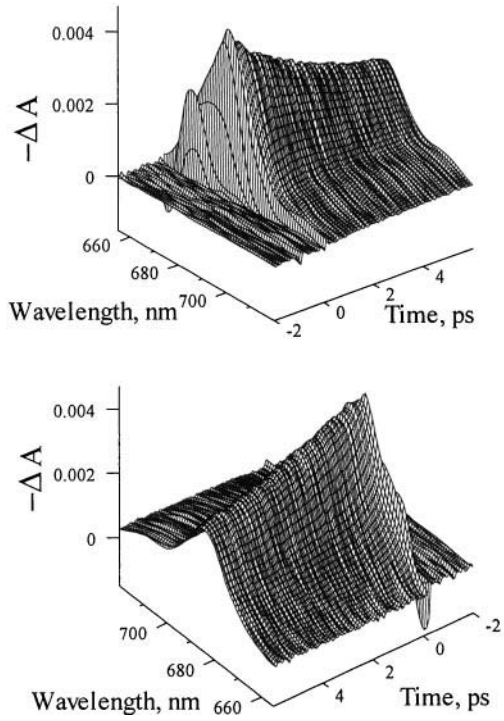

FIGURE 2 Two perspectives of the three-dimensional surface of ΔA versus time and probe wavelength for *Synechocystis* PS I trimers excited at 660 nm.

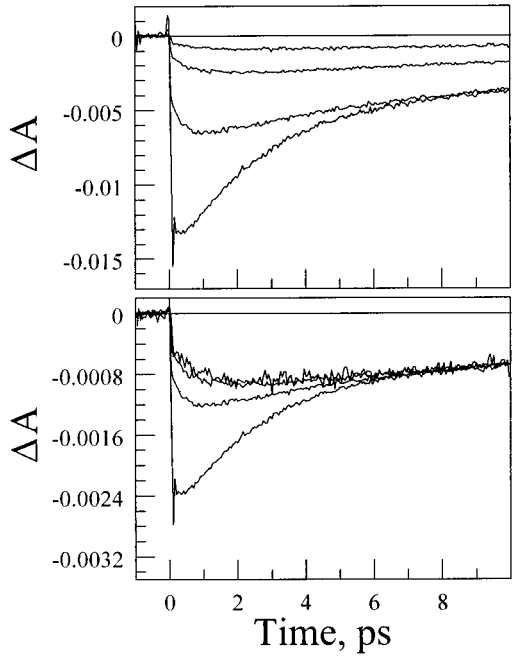

FIGURE 3 Pump-probe profiles for PS I excited at 660 nm and probed at 700 nm; successive pump powers are decreased by a factor of 2.5–3. Signal is dominated by PB/SE at all times. The top panel shows actual signals with absolute magnitudes; the bottom panel shows the same signals normalized together at long times. The vertical scale in the bottom panel corresponds to the signal for lowest pump power.

carried out with linear pump and probe polarizations separated by 54.7°. In anisotropy studies, the pump and probe polarizations were rapidly alternated between parallel and perpendicular using a Meadowlark Optics LRC-200-IR1 liquid crystal variable retarder (Longmont, CO); the optical anisotropy was then computed from the respective absorption difference signals $\Delta A_{\parallel}(t)$, $\Delta A_{\perp}(t)$ via $r(t) = (\Delta A_{\parallel}(t) - \Delta A_{\perp}(t))/(\Delta A_{\parallel}(t) + 2\Delta A_{\perp}(t))$.

RESULTS

Annihilation

The pump laser power dependence of absorption difference signals in wild-type PS I trimers was studied to ensure that experiments were carried out under annihilation-free conditions. Typical results are given in Fig. 3, which shows ΔA profiles excited by 660 nm frequency-doubled OPA pulses and probed by continuum pulses viewed at 700 nm. This pump wavelength excites Chl pigments on the short-wavelength side of the bulk antenna Q_y spectrum. The signals here are dominated by photobleaching and stimulated emission (PB/SE) at all times. The pump power was successively reduced by factors of 2.5–3. The actual ΔA signals are shown with true optical density units in the top panel, while the bottom panel shows the same profiles normalized together at long times (20–40 ps). The curves for successive laser powers become congruent only for maximum ΔA signals ≤ 0.001, corresponding to excitation of one of every $\sim$120 pigments. This is on the order of the size of the PS I core antenna-reaction center complex ($\sim$300 Chls per trimer). Under these conditions, individual pump pulses contained $<$10 nJ, and the spot size was $\sim$100 μm. (However, published estimates of excitation densities—which are typically accurate to no better than an order of magnitude—should not be used as guidelines by other laboratories; a power dependence study like the one in Fig. 3 should always be performed to establish the annihilation-free regime.) Analysis of these profiles with a four-exponential decay law yields the optimized lifetimes and amplitudes shown in Table 1. The amplitudes in this table are normalized to that of the longest-lifetime component (27–32 ps), which is somewhat longer than the 19–24 lifetimes previously attributed by Hastings et al. (1995) to trapping at the P700 reaction center in several cyanobacterial species. Two fits are listed for each pump power: one in which all lifetimes and amplitudes were freely varied, and one in which three of the lifetimes were frozen at the values 500 fs, 2.0 ps, and 12.0 ps. The latter values are close to the averages of the optimized lifetimes found in the free fits (with less weight given to the profile obtained at lowest power, which exhibited the lowest signal/noise). In either type of fit, the fourth lifetime shows little variation (30–32 ps except at the highest laser power, 27 ps). Since the standard deviations differ little between the two types of fits, there is little evidence that the component lifetimes vary with laser power; the metamorphosis in Fig. 3 arises primarily from amplitude redistribution. The amplitude of the 2-ps component changes sign from +2.1 to −0.53 when the power is reduced (Table 1, free fits). This is largely respon-

TABLE 1 Optimized parameters from multiexponential analysis of power-dependent 660 → 700 nm profiles for PS I from *Synechocystis*

Power	τ_1 (A_1)	τ_2 (A_2)	τ_3 (A_3)	τ_4 (A_4)	χ^2
8	0.21 (−0.89)	2.4 (2.1)	5.0 (−0.10)	27 (1.00)	1.13
	0.50 (−0.1)	**2.00** (2.6)	**12.0** (0.23)	30 (1.00)	1.17
4	0.55 (−1.27)	2.15 (0.66)	12.9 (1.14)	32 (1.00)	5.07
	0.50 (−1.2)	**2.00** (0.54)	**12.0** (1.00)	31 (1.00)	5.09
2	0.47 (−0.64)	1.74 (−0.43)	11 (0.84)	31 (1.00)	3.83
	0.50 (−0.80)	**2.00** (−0.40)	**12.0** (1.01)	32 (1.00)	3.83
1	0.72 (−0.85)	6.4 (−0.53)	**12.0 (1.00)**	**31 (1.00)**	3.37
	0.50 (−0.80)	**2.00** (−0.66)	**12.0 (1.00)**	**31 (1.00)**	3.64

Boldface values indicate fixed parameters; lowest power corresponded to excitation of 1 Chl of ~200. All lifetimes are in picoseconds.

sible for the transformation of the early-time behavior of the 660 → 700 nm profiles in Fig. 3, in which 2 ps PB/SE decay kinetics at high power are supplanted by 2 ps PB/SE rise kinetics at low power. Considerable power dependence is also observed in the 500 fs component amplitudes (Table 1). The 12-ps component amplitude is relatively unaffected, except at the highest laser power. It is clear from Fig. 3 that excessive laser powers, while not necessarily affecting the global analysis lifetimes, drastically alter the decay-associated spectra.

Global analyses of ΔA profiles for other probe wavelengths under low pump power (see below) indicate that the 500-fs and 2-ps lifetimes are due to bulk spectral equilibration and bulk ↔ red equilibration, respectively. It then appears reasonable to assign the 500-fs and 2-ps components in Table 1 to annihilations in bulk and red Chls, respectively. The 2-ps component observed under higher excitation powers in Table 1 becomes supplanted by a 6.4 ps component at the lowest power. The latter lifetime resembles one that emerges in global analyses of two-color profiles excited at 660 nm under low power (see below). Our global analyses yield no 12 ps component similar to that in Table 1, although similar components have appeared in analyses of individual pump-probe profiles (Lin et al., 1992) and fluorescence decays (Holzwarth et al., 1993; Turconi et al., 1993) of PS I core particles from *Synechococcus*.

Primary processes under annihilation-free conditions

Fig. 4 shows decay-associated spectra from global analyses of ΔA profiles obtained by exciting wild-type PS I trimers at 660 nm and probing at 5-nm intervals from 655 to 710 nm and at 720 nm (cf. Fig. 2). A global analysis with four freely varied lifetimes (hereafter termed the *g*4 analysis) yielded DAS components with lifetimes 400 fs, 4.8 ps, 22 ps, and 10,400 ps. The latter component exhibited very low amplitude in fresh PS I samples (cf. Fig. 4); its amplitude increased under exposure to the laser beams, and it likely arises from uncoupled Chls that cannot transfer excitation. The 4.8- and 22-ps lifetimes resemble the lifetimes 2.7–4.3 ps (*Synechocystis*) and 19–24 ps (cyanobacteria, green algae, and higher green plants) measured by Hastings et al. (1995).

Under present signal/noise, considerably more accurate fits were obtained in a *g*5 global analysis using five instead of four freely varied lifetimes. Their optimal values were 430 fs, 2.0 ps, 6.5 ps, 24 ps, and 10,800 ps. The statistical effects of splitting the 4.8-ps component into 2.0- and 6.5-ps components were tested by accumulating separate two-color profiles excited at 680, 710, and 716 nm (Table 2). Each profile was analyzed individually with four protocols: 1) four freely varied lifetimes and amplitudes (*f*4); 2) four

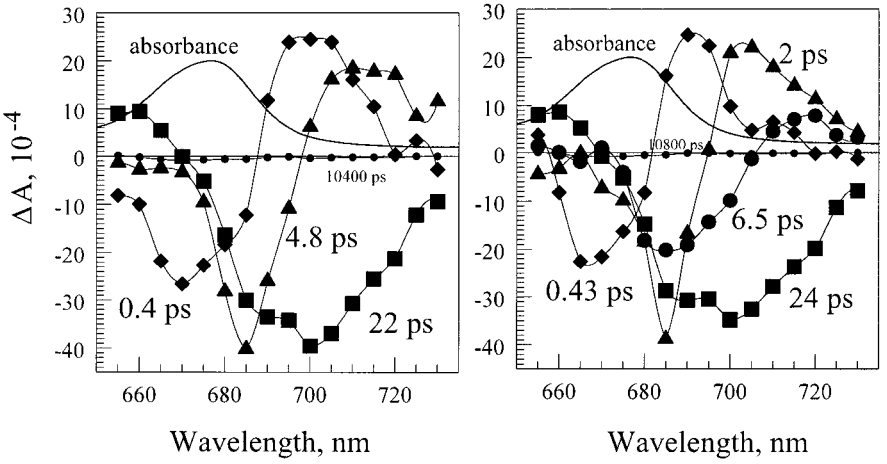

FIGURE 4 Decay-associated spectra from global analyses of ΔA surfaces for PS I excited at 660 nm: (*left*) *g*4 analysis with four freely varied lifetimes and amplitudes; (*right*) *g*5 analysis with five lifetimes and amplitudes. Positive and negative amplitudes correspond to PB/SE decay and rise components, respectively.

TABLE 2 Comparisons of *f*4, *g*4′, *g*5′, and *g*5″ multiexponential analyses for two-color profiles excited at 680, 710, and 716 nm

	τ_1 (A_1)	τ_2 (A_2)	τ_3 (A_3)	τ_4 (A_4)	Long (A_5)	χ^2
710 → 680 nm						
*f*4	0.24 (−0.68)	1.9 (−0.73)	—	27 (0.99)	(0.002)	2.39
*g*4′	0.44 (−0.77)	4.8 (−0.52)	—	22 (0.98)	(0.02)	2.63
*g*5′	0.43 (−0.61)	2.0 (−0.45)	6.5 (−0.20)	24 (0.98)	(0.02)	2.49
*g*5″	0.43 (−0.48)	2.0 (−0.75)	—	24 (0.98)	(0.02)	2.55
710 → 705 nm						
*f*4	0.02 (0.21)	0.74 (0.17)	2.0 (0.02)	17 (0.56)	—	6.65
*g*4′	0.44 (0.22)	4.8 (0.19)	—	22 (0.59)	(−0.03)	5.34
*g*5′	0.43 (0.17)	2.0 (0.10)	6.5 (0.17)	24 (0.56)	(−0.04)	5.33
*g*5″	0.43 (−0.03)	2.0 (0.35)	—	24 (0.65)	(−0.05)	5.82
710 → 710 nm						
*f*4	1.2 (−0.37)	2.2 (0.55)	—	28 (0.45)	—	1.10
*g*4′	0.44 (0.04)	4.8 (0.23)	—	22 (0.70)	(0.04)	1.19
*g*5′	0.43 (−0.44)	2.0 (0.44)	6.5 (−0.06)	24 (0.54)	(0.01)	1.14
*g*5″	0.43 (−0.23)	2.0 (0.37)	—	24 (0.61)	(0.02)	1.15
716 → 705 nm						
*f*4	0.04 (−0.97)	2.8 (0.38)	—	22 (0.60)	(0.02)	1.74
*g*4′	0.44 (0.19)	4.8 (0.26)	—	22 (0.53)	(0.02)	1.90
*g*5′	0.43 (0.06)	2.0 (0.22)	6.5 (0.18)	24 (0.53)	(0.02)	1.69
*g*5″	0.43 (−0.09)	2.0 (0.43)	—	24 (0.56)	(0.01)	2.30
680 → 710 nm						
*f*4	0.61 (−0.52)	3.1 (−0.55)	—	25 (1.00)	(0.002)	3.14
*g*4′	0.44 (−0.54)	4.8 (−0.55)	—	22 (0.99)	(0.01)	3.86
*g*5′	0.43 (−0.30)	2.0 (−0.47)	6.5 (−0.20)	24 (0.99)	(0.004)	3.04
*g*5″	0.43 (−0.18)	2.0 (−0.80)	—	24 (0.99)	(0.01)	4.03

All lifetimes are in picoseconds.

lifetimes (fixed at the *g*4 values) with varied amplitudes (*g*4′); 3) five fixed lifetimes from the *g*5 analysis with varied amplitudes (*g*5′); and 4) four components with lifetimes frozen at the *g*5 values, but excluding the 6.5-ps component (*g*5″). As judged by χ^2, the *g*4 protocol yielded poor fits (Table 2). Omitting the 6.5-ps component worsened the fits considerably, since this table shows that the *g*5″ fits are invariably poorer than the *g*5′ fits. Fig. 5 illustrates (for the case of the 660 → 700 nm profile) the marked improvement achieved by the *g*5 global analysis over the *g*4 analysis. In this example, the optimized *g*4 parameters could not reproduce the combined rise and decay features in the 660 → 700 nm profile during the first 8 ps. However, the *g*5 model mimics this behavior well.

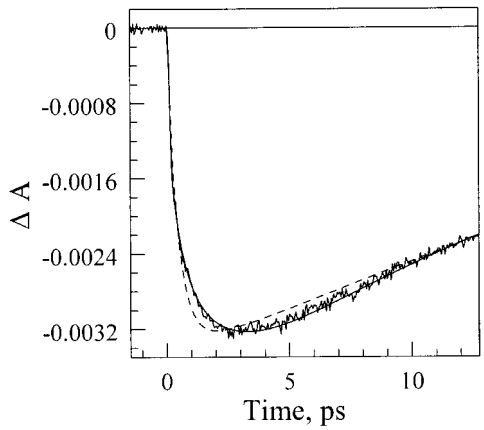

FIGURE 5 Comparison of experimental 660 → 700 nm profile with model profiles computed using optimized *g*4 parameters (*dashed curve*) and *g*5 parameters (*solid curve*).

These χ^2 tests establish the existence of more than one lifetime (or a distribution of lifetimes) in the neighborhood of 2 and 6.5 ps. The corresponding DAS of these components in Fig. 4 are quite different, with positive (growth) maxima at ~705 and 720 nm, respectively. The difference between these two DAS lies well outside our signal/noise ratio; equilibration between the bulk antenna and the red Chls is multiphasic. Postulating the existence of at least two distinct red Chl spectral forms with PB/SE maxima near 705 and 720 nm (in contrast to Gobets et al., 1994) would obviously account for these features, but this is not the only possible explanation (see below).

The sigmoidal 430-fs DAS in Fig. 4 arises from downhill spectral equilibration between bulk Chl forms with PB/SE maxima at ~665 and ~690 nm. This is perhaps the clearest perspective to date on subpicosecond bulk redistribution. The shape of the 24-ps DAS is of particular interest. While it exhibits considerable PB/SE decay amplitude in the red antenna Chl spectral region (>700 nm), it also shows an intense shoulder at 685–690 nm, overlapping the positive segment of the 430-fs DAS. (This structure in the ~20 ps DAS is less evident in earlier work under lower signal/noise, which tends to represent this DAS as broad and featureless.) Hence, the long-time decay kinetics in the red portion of the bulk antenna (like those in the red Chls) are dominated by ~24 ps decay in our global picture. (This

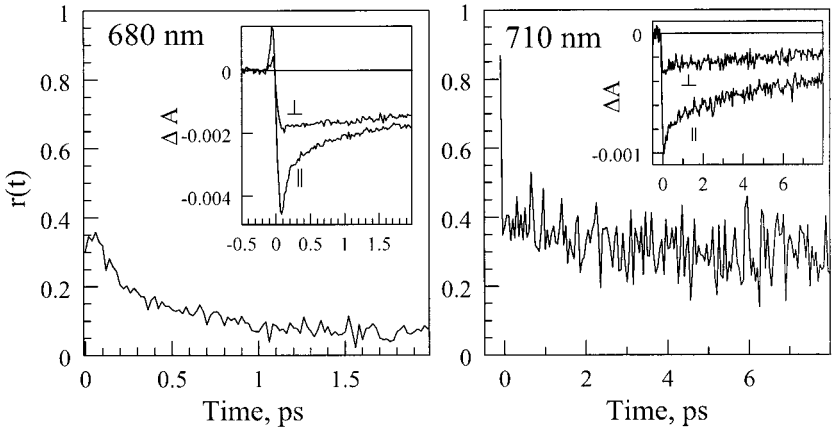

FIGURE 6 Polarized one-color pump-probe profiles and anisotropies $r(t)$ at 680 nm (*left*) and 710 nm (*right*). Positive and negative ΔA signals are dominated by PB/SE and ESA, respectively.

long-lived bulk excitation is qualitatively obvious in the 3-dimensional ΔA surface in Fig. 2). Bulk → red antenna transfers are thus not irreversible; a quasiequilibrium is reached among the red Chls and the bulk antenna. Similar conclusions have been already voiced by others (e.g., Owens et al., 1988; Holzwarth et al., 1990; Werst et al., 1992; Hastings et al., 1995).

Anisotropies

The contrast observed between anisotropy decays in the bulk and red Chls is illustrated for the 680- and 710-nm one-color experiments in Fig. 6. A single-exponential fit to the 680-nm anisotropy under annihilation-free conditions yields 590 fs decay time, with final anisotropy $r(\infty) = 0.07$; the initial anisotropy is nominally 0.27, suggesting that an additional, faster component may contribute to the overall anisotropy decay. This timescale resembles the lifetime of the bulk antenna spectral equilibration component in the $g4$ and $g5$ global analyses. This anisotropy decay is accelerated slightly (to 430 fs, not shown) when the laser power is increased threefold. The 710-nm anisotropy initializes near 0.4, and decays to $r(\infty) \sim 0.21$ with ~3.1-ps kinetics. In general, the red antenna Chls reach larger residual anisotropies $r(\infty)$ at long times, with slower decays. This is shown in Table 3, which tabulates optimized parameters from single-exponential fits to several one- and two-color anisotropies.

TABLE 3 Optimized parameters from single-exponential fits to anisotropies

$$r(t) = [r(0) - r(\infty)]e^{-t/\tau} + r(\infty)$$

Pump → Probe	τ	$r(\infty)$	$r(0)$
680 → 680	0.59	0.07	0.20
680 → 710	0.60	0.03	0.39
710 → 680	2.4	−0.04	−0.48
710 → 705	5.5	0.16	0.36
710 → 710	3.1	0.21	0.40
716 → 705	9.1	0.14	0.34

All lifetimes are in picoseconds.

An intriguing anisotropy is the 710 → 680 nm two-color profile in Fig. 7. In this case, the prompt anisotropy $r(0)$ is *negative* (unlike the 710-nm one-color anisotropy), because $\Delta A_{\parallel}$ and $\Delta A_{\perp}$ are dominated by ESA and PB/SE at early times, respectively. These signs suggest the presence of strongly interacting pigments with exciton components near 710 and 680 nm, because the prompt PB created at 680 nm is polarized nearly perpendicular to the transition moment excited at 710 nm. The initial anisotropy in the 716 → 680 nm experiment (not shown) is similarly negative.

DISCUSSION

Our most compelling result is the emergence of two distinct DAS components with lifetimes 2 and 6.5 ps for bulk → red energy transfers. Their growth peak positions nominally reflect energy transfers to red Chls absorbing at ~705 and 720 nm, respectively (cf. Fig. 4). It is unclear from our

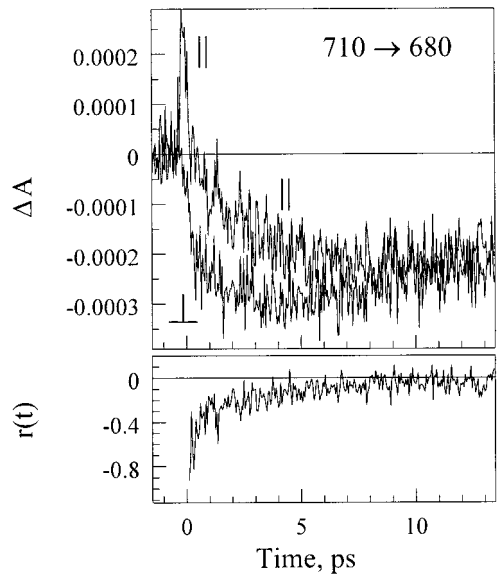

FIGURE 7 Polarized pump-probe profiles and anisotropy for 710 → 680 nm two-color experiment. Positive and negative ΔA signals are dominated by PB/SE and ESA, respectively.

analyses a priori whether these lifetimes correspond to discrete red Chls absorbing near the respective wavelengths, or whether they stem from a continuous distribution of lifetimes for energy transfers to a single, inhomogeneously broadened Chl form.

Gobets et al. (1994) encountered a similar issue when interpreting site-selected fluorescence studies of PS I core antenna-reaction center particles from *Synechocystis* sp. PCC 6803 at 4 K. (Our preparations appear to have been identical to theirs, aside from the absence of "free" Chls. Our samples showed similar steady-state fluorescence spectra peaking in the neighborhood of 720 nm (not shown); but they did not exhibit a 670-nm steady-state fluorescence band when excited at shorter wavelengths.) These authors reasoned that the red Chls in *Synechocystis* sp. exhibit a composite absorption maximum near 708 nm at 4 K, because the emission band maximum (718.5 nm) excited at this wavelength coincided with the band maximum observed under nonselective excitation. For other excitation wavelengths, the emission peak position (717–725 nm) correlated almost linearly with excitation wavelength between 702 and 720 nm. The 200 cm^{-1} Stokes' shift between the mean emission peak ($\sim$718 nm) and the absorption peak appeared to be unprecedentedly large for monomeric Chl *a*. Hence, the authors invoked a Q_y reorganization energy of $\sim$100 cm^{-1}, similar to that observed for dimeric BChl in the B820 subunit of LH1 (Pullerits et al., 1994) and in purple bacterial reaction centers (Reddy et al., 1992). This was rationalized by assigning the 708-nm absorption peak to a dimeric Chl *a* species. The emission peak position's sensitivity to excitation wavelength was attributed to inhomogeneous broadening. From an analysis of the emission peak's tracking of the excitation wavelength, it was concluded that the inhomogeneous broadening in the C708 Chls (215 cm^{-1}) was comparable to the homogeneous broadening (170 cm^{-1}). This treatment presumed the existence of only one red Chl species a priori; the presence of additional Chl forms at longer wavelengths appears not to have been explicitly considered. We will not judge the plausibility of these conclusions here, except to point out that similar tracking behavior would be observed in the emission spectra for multiple discrete, inhomogeneously broadened Chl spectral forms (e.g., C708 and C720). However, a single inhomogeneously broadened C708 species (like two discrete Chl species) would produce dispersive bulk $\leftrightarrow$ red equilibration kinetics, owing to variations in donor-acceptor spectral overlap.

The location and function of the red Chls in the PS I core complex have long intrigued photosynthesis workers. Indirect evidence (based on lattice model simulations of PS I core antenna kinetics, combined with temperature dependence of photon counting fluorescence profiles) suggested that (some of) the red Chls are positioned near the reaction center (Owens et al., 1988; Werst et al., 1992; Jia et al., 1992). Fluorescence spectra of PS I from *Spirulina platensis* and simulations of energy equilibration in *Synechocystis* sp. have recently suggested that far-red Chls are located on the periphery of PS I, perhaps in region(s) of contact between PS I monomers (Karapetyan et al., 1997; Gobets et al., 1998). Our group has analyzed room-temperature steady-state absorption spectra and 77 K fluorescence spectra for differences between wild-type PS I from *Synechocystis* sp. PCC 6803 and several of its subunit-deficient mutants (Soukoulis et al., 1999). The low-temperature fluorescence spectra of PS I mutants lacking one or more of the peripheral subunits PsaF/J, PsaI/L, PsaK, and PsaM are all essentially identical to the wild-type spectrum (whose main band near 720 nm is dominated by red Chls). Hence, the red Chls are intact in these mutants, and they are not bound to any of the deleted subunits. The absorption spectra of mutants lacking the PsaL and PsaM subunits (which bind several antenna Chls according to the electron density map of Krauss et al., 1996) appear to be deficient in red Chls absorbing near 700 nm at room temperature. In contrast, three other subunits on the edges of PsaA/B heterodimer (PsaF/J and PsaK) appear to bind small numbers of bluer Chls (685 nm and 665, 680 nm, respectively). The other subunit-deficient spectra are consistent with an essentially random spatial distribution of bulk Chl spectral forms. We caution here that these interpretations of our subunit-deficient mutant absorption spectra tacitly assume that Chls bound to undeleted subunits are unaffected by the mutation; this may not be strictly true. In any case, the red Chls responsible for the low-temperature fluorescence in *Synechocystis* sp. PCC 6803 (Gobets et al., 1994) are almost certainly bound to the PsaA/B heterodimer. The issue of whether they are peripheral or proximate to the reaction center is unresolved.

We have constructed kinetic models that combine cartoons of the bulk antenna topology with variously placed red Chls. Two of the models presume the existence of two discrete red Chl forms C_{705}, C_{720} responsible for the DAS components with growth peaks at 705 and 720 nm (Figs. 8–10). A third model does not. We thus leave open the question of whether the red Chls comprise more than one pigment in the electron density map, or whether they represent subpopulations of a single inhomogeneously broadened Chl type. No attempt was made to model the 430-fs intrabulk spectral equilibration, and no spectral differentiation was made among bulk Chls (hereafter denoted *B*); our focus was on the equilibration among Chl types *B*, C_{705}, and C_{720}. Either half of the bulk antenna was represented by 11 pigments arrayed on a semicircle. The number *N* of these pigments appears immaterial, since the intrabulk transfer rates can be adjusted to compensate for changes in *N* in order to match the experimental kinetics. To incorporate the approximate C_2 symmetry of the PsaA/B heterodimer (and to allow for energy transfer from the bulk pigments on the ends of the semicircle in Figs. 8 and 10 to the other side of the heterodimer), energy transfers from these terminal bulk pigments to their nearest neighbors occurred at twice the rate of transfers between other bulk pairs. Non-nearest neighbor energy transfers were ignored. The relevant kinetic equations were solved using Maple V.3 software for

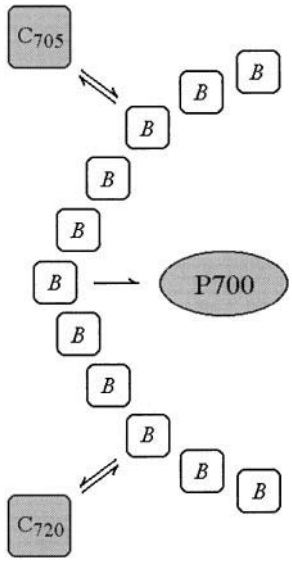

FIGURE 8 Model 1 for primary processes in photosystem I. White squares labeled *B* represent bulk Chls; optimized rate constants are given in text.

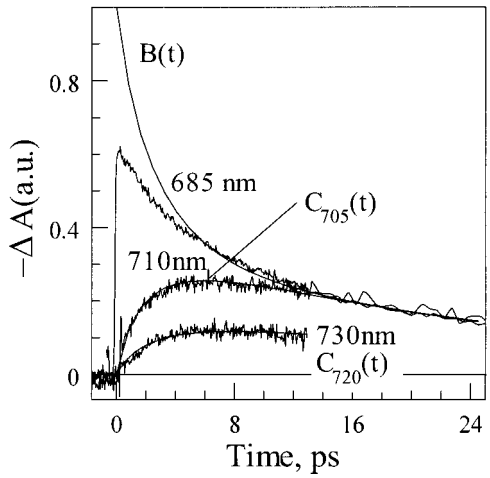

FIGURE 9 Simulated populations $B(t)$, $C_{705}(t)$, and $C_{720}(t)$ for uniform excitation of bulk antenna in model 1, superimposed on experimental two-color profiles excited at 660 nm and probed at 685, 710, and 730 nm. The contrasting PB/SE rise behavior observed in the latter two experimental profiles underscores the need for at least two lifetimes (2.0 and 6.5 ps in the *g*5 analysis) when describing the bulk ↔ red equilibration.

given rate constants, yielding numerical time-dependent populations for each of the three pigment types. Each population was in turn fitted with a biexponential rate law for comparison to empirical *g*5 lifetimes.

In model 1 (Fig. 8), the red Chls C_{705} and C_{720} equilibrate with peripheral bulk Chls; trapping at P700 occurs with rate k_T from a proximate bulk pigment. For uniform excitation of all bulk pigments, this model successfully replicated the bulk ↔ red equilibration kinetics using the rate constants $k_{B\rightarrow B} = (200\ \text{fs})^{-1}$, $k_{B\rightarrow C_{705}} = (450\ \text{fs})^{-1}$, $k_{C_{705}\rightarrow B} = (3.3\ \text{ps})^{-1}$, $k_{B\rightarrow C_{720}} = (8\ \text{ps})^{-1}$, $k_{C_{720}\rightarrow B} = (17\ \text{ps})^{-1}$, and $k_T = (1\ \text{ps})^{-1}$. The resulting C_{705} and C_{720} populations agree well with the experimental profiles obtained by probing at 710 and 730 nm, respectively (Fig. 9). The agreement with the bulk antenna kinetics is considerably less good; the simulated bulk excitation population decays more rapidly at early times than the experimental profile probed at 685 nm. This discrepancy is mitigated if some C_{705} absorption contributes to the total signal observed at 685 nm. The dimensionality and topology of our bulk antenna model (e.g., dimensionality and lack of non-nearest neighbor energy transfers) and our neglect of bulk heterogeneity (and its effects on spectral overlap) may well introduce artifacts here. Most of the rate constants in this model appear physically reasonable; for example, the 200-fs intrabulk energy transfers are of the same order as fluorescence depolarization times reported by Du et al. (1993), and the ratio of rate constants for the $C_{705} \rightarrow B$ and $B \rightarrow C_{705}$ steps is commensurate with the expected Boltzmann factor (0.14) for energy transfers between Chls absorbing at 685 and 705 nm. However, the equilibration steps involving C_{720} appear to be unphysically slow, and the ratio of up to downhill rates involving C_{720} (0.47) is much larger than the pertinent Boltzmann factor (0.03). In this model, such low values for $k_{B\rightarrow C_{720}} = (8\ \text{ps})^{-1}$, $k_{C_{720}\rightarrow B} = (17\ \text{ps})^{-1}$ are needed to mimic the 6.5-ps PB/SE rise kinetics observed at the longest wavelengths. These rate constants also force the C_{720} population to decay with 37-ps kinetics, rather than the observed 24 ps. In this simulation, the long-time decay kinetics are not uniform among the three populations: 25 ps for *B*, 22 ps for C_{705}, and 37 ps for C_{720}.

In a second model (model 2), excitation is channeled to the reaction center via red pigments C_{705} and C_{720}; the former is coupled to a proximate bulk Chl, as shown in Fig. 10. Excitation on C_{720} can be trapped at P700. (This sequence will certainly not describe the trapping at low temperatures; under these conditions, excitations reaching C_{720} would remain confined there, and trapping from the bulk to

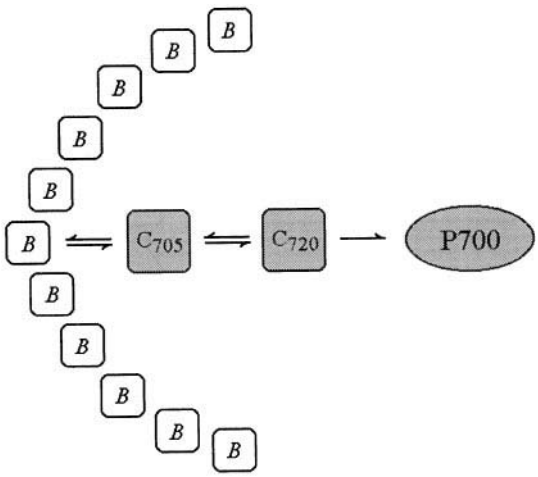

FIGURE 10 Model 2 for primary processes in photosystem I. White squares labeled *B* represent bulk Chls; optimized rate constants are given in text.

P700 would bypass C_{720}.) A set of rate constants that models the observed room-temperature kinetics well is $k_{B\rightarrow B} = k_{B_1\rightarrow C_{705}} = (200\ \text{fs})^{-1}$, $k_{C_{705}\rightarrow B_1} = (2.8\ \text{ps})^{-1}$, $k_{C_{705}\rightarrow C_{720}} = (12\ \text{ps})^{-1}$, and $k_T = (3\ \text{ps})^{-1}$. The ratio $k_{B_1\rightarrow C_{705}}/k_{C_{705}\rightarrow B_1}$ obeys detailed balancing of 680- and 708-nm Chls; by similar reasoning, the rate $k_{C_{720}\rightarrow C_{705}}$ for energy transfers from C_{720} to C_{705} would be so slow as to have little influence on the overall kinetics. For uniform excitation of all 11 bulk pigments in model 2, the bulk antenna decay $B(t)$ could be fit with 2- and 22-ps kinetics (48% and 52%, respectively). Biexponential fits to the $C_{705}(t)$ showed 1.9 ps rise and 22.6 ps decay kinetics; $C_{720}(t)$ showed 6.6-ps rise and 17.6-ps decay kinetics. These lifetimes resemble the *g*5 component lifetimes 2.0 ps, 6.5 ps, and 24 ps. The ~20-ps trapping lifetime is not truly uniform over bulk and red populations as represented in the *g*5 analysis. The 2-ps lifetime arises from a trajectory-averaged sequence of 200-fs energy transfer steps; the 6.6-ps component stems in part from a 12-ps $C_{705} \rightarrow C_{720}$ bottleneck. The three populations $B(t)$, $C_{705}(t)$, $C_{720}(t)$ simulated in model 1 agree well with the experimental two-color profiles 660 → 685, 660 → 710, and 660 → 730 nm (not shown). At these wavelengths, the absorption difference signal is presumably dominated by PB/SE from bulk Chls, C_{705}, and C_{720}, respectively. While most of the rate constants in this model seem physiological, the slow 12-ps kinetics for the downhill $C_{705} \rightarrow C_{720}$ step appear difficult to explain.

In model 3 (not shown), a single red Chl species is coupled to a peripheral bulk Chl; dispersion in the bulk ↔ red equilibration kinetics arises from an inhomogeneous distribution of red Chl site energies. Such a model can easily yield equilibration kinetics as disparate as 2 and 6.5 ps using reasonable rate constants, because the Boltzmann factors for uphill energy transfers to 685-nm bulk pigments from 705- and 720-nm Chls differ by a factor of ~4. Model 3 differs from model 1, where the rapid intrabulk energy transfers cause the bulk ↔ C_{705} and bulk ↔ C_{720} equilibrations to be strongly coupled. (Equilibrations between the bulk and the various red Chl subpopulations within an inhomogeneously broadened red spectrum in model 3 would of course be uncoupled.) This coupling considerably reduces the flexibility in model 1, where it was necessary to postulate the implausible rate constants $k_{B\rightarrow C_{720}} = (8\ \text{ps})^{-1}$, $k_{C_{720}\rightarrow B} = (17\ \text{ps})^{-1}$ in order to simulate the observed 6.5-ps rise kinetics.

To ascertain whether such inhomogeneous broadening would realistically produce biexponential bulk ↔ red equilibration kinetics (with lifetimes that bracket the continuous distribution) in a global analysis, we generated time-dependent profiles that combined 2- and 6-ps PB risetime components with a 24-ps decay component. The amplitudes of the respective rise components were modeled for each probe wavelength using 13-nm fwhm Gaussians centered at 708 and 720 nm. Gaussian noise was superimposed on each of the profiles. Each profile could be fitted well with single-exponential rise behavior; the optimized risetimes varied continuously from 2.00 ps to 5.85 ps over the interval from 705 to 727.5 nm. Conversely, a global analysis will differentiate between (1) homogeneous single-exponential rise kinetics, and (2) a single-exponential rise feature with wavelength dispersion in its lifetime. A biexponential model will yield a better fit in the latter case under our signal/noise. (The same is not true for fitting an individual profile at a given probe wavelength; biexponential models will yield little improvement here over a single-exponential fit for risetimes as close together as 2 and 6 ps.)

In summary, model 3—in which the disperse bulk ↔ red equilibration kinetics arise from inhomogeneous broadening in a single red Chl species—more readily accounts for our observations than models 1 or 2. However, we emphasize that some of these conclusions may be artifacts of the models; the spectral diversity of the bulk antenna (which is not considered here) surely influences the overall kinetics. Reality-based simulations—using the full 4 Å x-ray structure of Krauss et al. (1996), combined with overlap factors computed from single-site Chl *a* absorption spectra randomly distributed in such a way as to replicate the steady-state absorption spectrum of photosystem I—are currently in progress (S. Savikhin and W. Struve, manuscript in preparation).

Given the size of the PS I core antenna-reaction center complex, even a *g*5 analysis cannot extract all of the key energy transfer and trapping features. In this context, the lack of consensus on PS I lifetimes and mechanisms (van Grondelle et al., 1994; Hastings et al., 1995) is understandable. According to the *g*5 decay-associated spectra in Fig. 4, the dominant lifetime components yielded by analysis of a particular two-color profile excited at 660 nm (the blue edge of the bulk antenna) will depend strongly on probe wavelength. For example, the 2- and 6.5-ps DAS amplitudes vanish at 690 and 710 nm, respectively. Separation of these two lifetimes (when they coexist in profiles at other wavelengths) requires higher signal/noise than previously available; the 2.7–4.3 ps component described by Hastings et al. (1995) may be a weighted mean of our 2- and 6.5-ps components. Our annihilation study (Table 1) also hints at the presence of a 12-ps component that does not turn up in our global analyses. The 8–12-ps bulk → red energy transfers reported by Holzwarth et al. (1993) and Turconi et al. (1993) for *Synechococcus* sp. may correspond to this 12-ps component. Finally, our simulations suggest that full bulk ↔ red equilibration is not reached in PS I, because the long decay lifetimes differ among the Chl forms. In such a case, the concept of global analysis will not apply to PS I.

The 430-fs *g*5 DAS component arising from spectral equilibration among bulk antenna pigments and the 590-fs bulk anisotropy decay at 680 nm are of the same order as the 150–300-fs fluorescence depolarization times observed by Du et al. (1993) in upconversion studies of the PS I core antenna from *Chlamydomonas reinhardtii*. The latter were ascribed to single-step energy transfer times. Our subpicosecond bulk spectral equilibration suggests that excitation deposited in a pigment at the blue edge of the bulk spectrum

will typically migrate downhill to 680–690-nm bulk pigments within one to three excitation hops.

The residual one-color anisotropy at 680 nm ($r(\infty) = 0.07$, $\tau = 590$ fs) is consistent with near-random orientations of bulk pigments; linear dichroism experiments also suggest that bulk antenna pigments are essentially randomly oriented (Tapie et al., 1984). The much larger residual anisotropy at 710 nm ($r(\infty) = 0.28$) is characteristic of energy transfers among preferentially oriented red pigments. The slow time scale of the one-color anisotropy for red Chls (3.1 ps at 710 nm, Table 3) is interesting, because it suggests energy transfers between red Chls separated by at least ~20 Å. If this stems from equilibration between rotationally equivalent red pigments in a PS I trimer, the anisotropy decay would show kinetics accelerated by a factor of 3 over the energy transfer rate constant (Lyle and Struve, 1991). In this case, the 3.1-ps anisotropy decay would correspond to 9.3-ps energy transfer kinetics between rotationally equivalent red Chls. However, the numbers and locations of the red Chls are not established, and the pertinent energy transfers may occur between red Chls bound to the same monomer.

We finally comment on the 710 → 680 nm anisotropy in Fig. 7. The negative initial anisotropy suggests that the pump and probe wavelengths lie near the lower and upper exciton components of a Chl dimer. Two candidates for such a dimer are (1) the dimeric Chls thought to be responsible for the C708 nm absorption band in *Synechocystis* (Gobets et al., 1994); and (2) the P700 special pair. The 2.4-ps anisotropy decay time seems commensurate with the 3.1-ps 710-nm one-color anisotropy decay associated with equilibration among red Chls. The kinetics of the charge transfer process P700* $A_0 \rightarrow P700^+ A_0^-$ are still unclear; the recent PS I energy transfer simulation of Gobets et al. (1998) models the charge separation with 620-fs kinetics. In neither case is the location of the upper exciton component known. For P700, Schaffernicht and Junge (1981) reported that the upper exciton component lies at ~695 nm; Vrieze et al. (1992) suggested ~650 nm. Brettel (1997) proposed that it lies ~18 nm to the blue of the lower component (i.e., at ~682 nm), using a simple exciton model. A study of absorption difference spectra between wild-type PS I and its reaction center site-directed mutants is in progress in our laboratory, and may shed light on this question.

The Ames Laboratory is operated for the U.S. Department of Energy by Iowa State University under contract No. W-7405-Eng-82. This work was supported in part by the Division of Chemical Sciences, Office of Basic Energy Sciences (to W.S.S.), and in part by National Science Foundation Grants MCB#9696170 and MCB#9723001 (to P.C.).

This is Journal Paper No. 18124 of the Iowa Agriculture and Home Economics Experiment Section, Ames, IA, Project No. 3416, supported by Hatch Act and State of Iowa funds.

REFERENCES

Brettel, K. 1997. Electron transfer and arrangement of the redox cofactors in photosystem I. *Biochim. Biophys. Acta.* 1318:322–373.

Buck, D. R., S. Savikhin, and W. S. Struve. 1997. Ultrafast absorption difference spectra of the Fenna–Matthews–Olson protein at 19 K. Experiment and simulations. *Biophys. J.* 72:24–36.

Du, M., X. Xie, Y. Jia, L. Mets, and G. R. Fleming. 1993. Direct observation of ultrafast energy transfer in PS I core antenna. *Chem. Phys. Lett.* 201:535–542.

Gobets, B., J. P. Dekker, and R. van Grondelle. 1998. Transfer-to-the-trap limited model of energy transfer in photosystem I. *Proceedings of the International Congress on Photosynthesis, Budapest, Hungary, August 1998.*

Gobets, B., H. van Amerongen, R. Monshouwer, J. Kruip, M. Rögner, R. van Grondelle, and J. P. Dekker. 1994. Polarized site-selected fluorescence spectroscopy of isolated photosystem I particles. *Biochim. Biophys. Acta.* 1188:75–85.

Hasson, K. C. 1997. Time-resolved studies of the protein bacteriorhodopsin using femtosecond laser pulses. Ph.D. thesis, Harvard University, Cambridge, MA.

Hastings, G., S. Hoshina, A. N. Webber, and R. E. Blankenship. 1995. Universality of energy and electron transfer processes in photosystem I. *Biochemistry.* 34:15512–15522.

Hecks, B., K. Wulf, J. Breton, W. Leibl, and H.-W. Trissl. 1994. Primary charge separation in photosystem I: a two-step electrogenic charge separation connected with $P700^+$ $A0^-$ and $P700^+$ A_1^- formation. *Biochemistry.* 33:8619–8624.

Holzwarth, A. R. 1991. Excited state kinetics in chlorophyll systems and its relationship to functional organization of the photosystems. *In* Chlorophylls. H. Scheer, editor. CRC Press, Boca Raton, FL. 1125–1151.

Holzwarth, A. R. 1992. Exciton dynamics in antennae and reaction centers of photosystems I and II. *In* Research in Photosynthesis, Vol. I. N. Murata, editor. Kluwer Academic Publishers, Dordrecht. 187–194.

Holzwarth, A. R., W. Haehnel, R. Ratajczak, E. Bittersmann, and G. H. Schatz. 1990. Energy transfer kinetics in photosystem I particles isolated from Synechococcus sp. and from higher plants. *In* Current Research in Photosynthesis. M. Baltscheffsky, editor. Kluwer Academic Publishers, Dordrecht. 611–614.

Holzwarth, A. R., G. H. Schatz, H. Brock, and E. Bittersmann. 1993. Energy transfer and charge separation kinetics in photosystem I. I. Picosecond transient absorption and fluorescence study of cyanobacterial photosystem I particles. *Biophys. J.* 64:1813–1826.

Ikegami, I., and S. Itoh. 1986. Chlorophyll organization in P-700-enriched particles isolated from spinach chloroplasts: CD and absorption spectroscopy. *Biochim. Biophys. Acta.* 851:75–85.

Jia, Y., J. M. Jean, M. M. Werst, C.-K. Chan, and G. R. Fleming. 1992. Simulations of the temperature dependence of energy transfer in the PS I core antenna. *Biophys. J.* 63:259–273.

Karapetyan, N. V., D. Dorra, G. Schweitzer, I. N. Bezsmertnaya, and A. R. Holzwarth. 1997. Fluorescence spectroscopy of the longwave chlorophylls in trimeric and monomeric photosystem I core complexes from the cyanobacterium *Spirulina platensis. Biochemistry.* 36:13830–13837.

Krauss, N., W. Hinrichs, I. Witt, P. Fromme, W. Pritzkow, Z. Dauter, C. Betzel, K. S. Wilson, H. T. Witt, and W. Saenger. 1993. Three-dimensional structure of system I of photosynthesis at 6 Å resolution. *Nature.* 361:326–330.

Krauss, N., W.-D. Schubert, O. Klukas, P. Fromme, H. T. Witt, and W. Saenger. 1996. Photosystem I at 4 Å resolution: a joint photosynthetic reaction center and core antenna system. *Nat. Struct. Biol.* 3:965–973.

Kwa, S. L. S., S. Völker, N. T. Tilly, R. van Grondelle, and J. P. Dekker. 1994. Polarized site-selection spectroscopy of chlorophyll *a* in detergent. *Photochem. Photobiol.* 59:219–228.

Lin, S., H. van Amerongen, and W. S. Struve. 1992. Ultrafast pump-probe spectroscopy of the P700- and FX-containing photosystem I core protein from *Synechococcus* sp. PCC 6301 (*Anacystis nidulans*). *Biochim. Biophys. Acta.* 1140:6–14.

Lyle, P. A., and W. S. Struve. 1991. Dynamic linear dichroism in chromoproteins. *Photochem. Photobiol.* 53:359–365.

Owens, T. G., S. P. Webb, L. Mets, R. S. Alberte, and G. R. Fleming. 1988. Antenna structure and excitation dynamics in photosystem I. I. Studies of detergent-isolated photosystem I preparations using time-resolved fluorescence analysis. *Biophys. J.* 53:733–745.

Pullerits, T., and V. Sundström. 1996. Photosynthetic light-harvesting pigment-protein complexes: toward understanding how and why. *Acc. Chem. Res.* 29:381–389.

Pullerits, T., F. van Mourik, R. Monshouwer, R. W. Visschers, and R. van Grondelle. 1994. Electron photon coupling in the B820 subunit form of LH1 studied by temperature dependence of optical spectra. *J. Lumin.* 58:168–171.

Reddy, N. R. S., P. A. Lyle, and G. J. Small. 1992. Applications of spectral hole burning spectroscopies to antenna and reaction center complexes. *Photosynth. Res.* 31:167–194.

Savikhin, S., Y. Zhu, S. Lin, R. E. Blankenship, and W. S. Struve. 1994. Femtosecond spectroscopy of chlorosome antennas from the green photosynthetic bacterium *Chloroflexus aurantiacus. J. Phys. Chem.* 98: 10322–10334.

Savikhin, S., P. I. van Noort, Y. Zhu, S. Lin, R. E. Blankenship, and W. S. Struve. 1995. Ultrafast energy transfer in light-harvesting chlorosomes from the green sulfur bacterium *Chlorobium tepidum. Chem. Phys.* 194:245–258.

Schaffernicht, H., and W. Junge. 1981. Analysis of the complex band spectrum of P700 based on photoselection studies with photosystem I particles. *Photochem. Photobiol.* 34:223–232.

Shubin, V. V., I. N. Bezsmertnaya, and N. V. Karapetyan. 1992. Isolation from *Spirulina* membranes of two photosystem I-type complexes one of which contains chlorophyll responsible for the 77 K fluorescence band at 760 nm. *FEBS Lett.* 309:340–342.

Soukoulis, V., S. Savikhin, W. Xu, P. R. Chitnis, and W. S. Struve. 1999. Electronic spectra of PSI mutants: the peripheral subunits do not bind red chlorophylls in Synechocystis sp. PCC 6803. *Biophys. J.* (in press).

Sun, J., K. An, P. Jin, V. P. Chitnis, and P. R. Chitnis. 1998. Isolation and characterization of photosystem I subunits from the cyanobacterium *Synechocystis* sp. PCC 6803. *Methods Enzymol.* 297:124–139.

Tapie, P., Y. Choquet, J. Breton, P. Delepelaire, and F.-A. Wollman. 1984. Orientation of photosystem I pigments: investigation by low-temperature linear dichroism and polarized fluorescence emission. *Biochim. Biophys. Acta.* 767:57–69.

Trinkunas, G., and A. R. Holzwarth. 1994. Kinetic modeling of exciton migration in photosynthetic systems. 2. Simulations of excitation dynamics in two-dimensional photosystem I core antenna/reaction center complexes. *Biophys. J.* 66:415–429.

Turconi, S., G. Schweitzer, and A. R. Holzwarth. 1993. Temperature dependence of picosecond fluorescence kinetics of a cyanobacterial photosystem I particle. *Photochem. Photobiol.* 57:113–119.

Van der Lee, J., D. Bald, S. L. S. Kwa, R. van Grondelle, M. Rögner, and J. P. Dekker. 1993. Steady-state polarized light spectroscopy of isolated photosystem I complexes. *Photosynth. Res.* 35:311–321.

Van Grondelle, R., J. P. Dekker, T. Gillbro, and V. Sundström. 1994. Energy transfer and trapping in photosynthesis. *Biochim. Biophys. Acta.* 1187:1–65.

Vrieze, J., P. Gast, and A. J. Hoff. 1992. The structure of the photosystem I reaction center investigated with linear dichroic absorbance-detected magnetic resonance at 1.2 K. *In* Research in Photosynthesis. N. Murata, editor. Kluwer Academic Publishers, Dordrecht. 553–556.

Vulto, S., A. M. Streltsov, and T. J. Aartsma. 1997. Excited state energy relaxation in the FMO complexes of the green bacterium *Prosthecochloris aestuarii* at low temperatures. *J. Phys. Chem. B.* 101:4845–4850.

Werst, M., Y. Jia, L. Mets, and G. R. Fleming. 1992. Energy transfer and trapping in photosystem I core antenna: a temperature study. *Biophys. J.* 61:868–878.